

Nonlinear eigenvalue problems for coupled Helmholtz equations modeling gradient-index graphene waveguides

Jung Heon Song^{a,1,2}, Matthias Maier^{b,1,3,*}, Mitchell Luskin^{a,1,2}

^a *School of Mathematics, University of Minnesota, 206 Church Street SE, Minneapolis, MN 55455, USA.*

^b *Department of Mathematics, Texas A&M University, 3368 TAMU, College Station, TX 77843, USA.*

Abstract

We discuss a quartic eigenvalue problem arising in the context of an optical waveguiding problem involving atomically thick $2D$ materials. The waveguide configuration we consider consists of a gradient-index (spatially dependent) dielectric equipped with conducting interior interfaces. This leads to a quartic eigenvalue problem with mixed transverse electric and transverse magnetic modes, and strongly coupled electric and magnetic fields. We derive a weak formulation of the quartic eigenvalue problem and introduce a numerical solver based on a *quadratisation approach* in which the quartic eigenvalue problem is transformed to a *spectrally equivalent* linear eigenvalue problem. We verify our numerical framework against analytical solutions for prototypical geometries. As a practical example, we demonstrate how an improved quality factor (defined by the ratio of the real and the imaginary part of the computed eigenvalues) can be obtained for a family of gradient-index host materials with internal conducting interfaces. We outline how this result lays the groundwork for solving related shape optimization problems.

Keywords: Guided mode, time-harmonic Maxwell's equations, surface plasmon polariton, nonlinear eigenvalue problem, quartic eigenvalue problem, quadratisation

2010 MSC: 65N30, 78M10, 78M30, 35P30

1. Introduction

Surface plasmon polaritons (SPPs) are charge density waves that are coupled to electromagnetic (EM) waves at the interface between a metal and a dielectric substrate. Exhibiting strong confinement and relatively low propagation losses, they are thought to be a novel way to confine and control light on the subwavelength scale in the field of nanophotonic technology. Such SPPs can be excited in graphene, a two-dimensional carbon allotrope with a single atom layer that is arranged in a honeycomb lattice structure [1]. It is characterized by strong confinement, low losses, and extreme tunability [1, 2]; In the infrared regime, the electric surface conductivity of such a 2D material is characterized by being complex-valued with a dominant positive imaginary part. This allows for the propagation of SPPs. Plasmons on graphene offer not only a lower ohmic loss than conventional plasmonic materials, but also a strong subwavelength confinement of the EM field [3, 4]. The tunability of graphene by electrical gating or chemical doping, makes graphene a promising candidate for future compact plasmon devices [5].

A conventional approach of analyzing a waveguide problem is to first reduce Maxwell's equations to a Helmholtz eigenvalue problem. For a homogeneously filled waveguide, the EM fields decouple from one another, making the numerical simulation straightforward. However, if spatially dependent material parameters (gradient-index materials) are introduced, the field components are no longer independent from each other, and we are left with a coupled *nonlinear eigenvalue problem*.

Computational approaches for solving nonlinear eigenvalue problems have been studied in the literature [6, 7, 8, 9]. They typically require specialized solvers not readily available in finite element [10] and numerical linear algebra toolkits [11, 12]. In this paper we pursue a different approach that allows to use existing linear algebra techniques. To that end, we investigate a general class of waveguide configurations that consist of spatially dependent material parameters and contain (arbitrarily shaped) interior conducting 2D material interfaces. In detail, our contributions are as follows:

*Corresponding author

Email addresses: `songx762@umn.edu` (Jung Heon Song), `maier@math.tamu.edu` (Matthias Maier), `luskin@umn.edu` (Mitchell Luskin)

¹The authors were supported in part by ARO MURI Award W911NF-14-1-0247.

²The first and third author's research was supported in part by NSF Awards DMS-1819220 and DMS-1906129.

³This author's research was supported in part by NSF Award DMS-1912847.

- We derive a variational, nonlinear quartic eigenvalue problem for a waveguiding problem incorporating spatially dependent material parameters and interior conducting interfaces (see Section 2.2). The nonlinear quartic character of the eigenvalue problem stems from the fact that the spatially dependent material parameters cause a strong coupling between the otherwise decoupled transverse magnetic (TM) and transverse electric (TE) modes (as would normally be the case for the Helmholtz equation).
- We solve the quartic eigenvalue problem numerically by transforming it to a spectrally equivalent linear system using a quadratification [13] approach. Additional numerical tools, such as the Möbius transform and a perfectly matched layer (PML) are employed to assist with solving the eigenvalue problem. We verify our numerical method against analytical solutions for prototypical geometries with internal conducting interfaces.
- As a practical example, we demonstrate how an improved quality factor (defined by the ratio of the real and the imaginary part of the computed eigenvalues) can be obtained (a) for a family of gradient-index host materials, and (b) by deformation of the geometry (see Section 5.3). Finally, we outline how our framework lays the groundwork for solving related shape optimization problems.

1.1. Related works

Optical properties of cylindrical waveguides with graphene interfaces have been extensively studied in the engineering community [3, 14, 15, 16]. Recently, focus has also shifted to gradient-index structures that couple with graphene [17, 18]. These structures are based on planar and cylindrical graphene-dielectric multilayer metamaterials, and have shown potential applications in terahertz imaging, sensing, detecting, and communication areas [17, 18]. Numerical methods that compute eigenvalues of inhomogeneously loaded domains have been studied before [19, 20, 21, 22]. A finite difference frequency-domain method is used to analyze eigenmodes of inhomogeneously loaded rectangular waveguides in [19]. Another study [22] presents a method for computing solenoidal eigenmodes and the corresponding eigenvalues of the vector Helmholtz equation. However, neither of these references take into account possible conducting interfaces.

There exist a number of methods for numerically solving nonlinear eigenvalue problems. The FEAST algorithm [23, 6] uses complex contour integration to compute a cluster of eigenvalues within some user-defined region in

the complex plane. Studies have also used the algorithm to simulate propagation of light through optical fibers [7, 8]. Another technique is within the context of Rayleigh quotient optimization problem [9], where a nonlinear eigenvalue problem is solved using a spectral transformation based on nonlinear shifting and a reformulation using second-order derivatives. In this paper, however, a different method based on *quadratisation* is proposed that is both pragmatic and applicable to a wide range of optical waveguiding problems.

1.2. Paper organization

The remainder of the paper is organized as follows. In Section 2, we derive a variational quartic eigenvalue problem for the waveguiding problem based on time-harmonic Maxwell's equations. In Section 3, we describe our numerical approach for solving the quartic eigenvalue problem, including a linearization based on quadratisation, the use of a Möbius transform to shift the spectrum, and a PML. Section 4 discusses and derives analytical solutions for prototypical configurations, which will be used to verify our numerical method in the subsequent section. Section 5 presents numerical results in domains with and without azimuthal symmetry. We demonstrate how our numerical method can be extended to arbitrary computational domains. Section 6 concludes the paper with a summary of our results and an outlook.

2. Variational formulation

We introduce a variational formulation for a relevant eigenvalue problem prescribed with a gradient-index host material with (arbitrarily shaped) conducting interfaces in the context of a waveguide configuration. A convenient rescaling of the equations to dimensionless forms is used [24].

2.1. Preliminaries

The source-free time-harmonic Maxwell's equations are given by

$$(1) \quad \begin{cases} \nabla \times \mathbf{E} &= i\omega\mu\mathbf{H}, \\ \nabla \times \mathbf{H} &= -i\omega\varepsilon\mathbf{E}, \end{cases}$$

where $\mathbf{E}(\mathbf{x})$ and $\mathbf{H}(\mathbf{x})$ denote the electric and magnetic field, respectively, and ω is the temporal frequency. $\mu(x, y)$ and $\varepsilon(x, y)$ are complex-valued

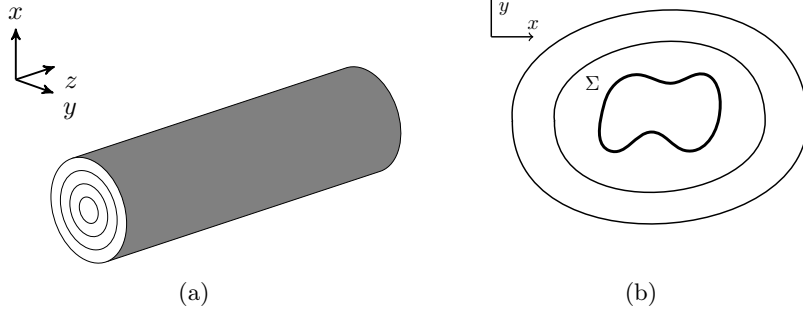


Figure 1: (a) Schematic of a prototypical multilayer waveguide. (b) Cross-sectional schematic of the computational domain. The closed curve, Σ , is prescribed with a non-vanishing conductivity. The waveguide is characterized by material parameters $\varepsilon(x, y)$ and $\mu(x, y)$.

functions of the transverse coordinates, where μ denotes the magnetic permeability and ε denotes the electric permittivity. In order to study *guided modes* we make the additional ansatz

$$\mathcal{F} \sim e^{ik_z z},$$

and decompose the fields $\mathcal{F} = \{\mathbf{E}, \mathbf{H}\}$ and the gradient operator, ∇ , into their longitudinal and transverse parts, whence we obtain

$$\mathcal{F} = \mathcal{F}_s + \hat{z}\mathcal{F}_z, \quad \nabla = \nabla_s + ik_z \hat{z},$$

where the subscript s denotes the transverse direction and \hat{z} denotes the unit vector in z -direction. In the strong sense, (1) holds true everywhere except on the points comprising the conducting interface, Σ . The surface conductivity $\sigma^\Sigma(x, y)$ on the conducting interface Σ gives rise to a jump condition on the tangential part of the magnetic field [24]. In summary, we obtain

$$(2) \quad \begin{cases} [\boldsymbol{\nu} \times (\mathbf{H}_s + \hat{z}H_z)]_\Sigma = \sigma^\Sigma (\boldsymbol{\nu} \times (\mathbf{E}_s + \hat{z}E_z)) \times \boldsymbol{\nu}, \\ [\boldsymbol{\nu} \cdot \mu(\mathbf{H}_s + \hat{z}H_z)]_\Sigma = 0, \\ [\boldsymbol{\nu} \times (\mathbf{E}_s + \hat{z}E_z)]_\Sigma = 0, \\ [\boldsymbol{\nu} \cdot \varepsilon(\mathbf{E}_s + \hat{z}E_z)]_\Sigma = \frac{1}{i\omega} \nabla \cdot (\sigma^\Sigma \mathbf{E}), \end{cases}$$

where $\boldsymbol{\nu}$ is a chosen unit normal vector field on Σ , and $[\cdot]_\Sigma$ denotes the jump over Σ with respect to $\boldsymbol{\nu}$, viz.,

$$[\mathbf{F}]_\Sigma(\mathbf{x}) := \lim_{\alpha \searrow 0} \left(\mathbf{F}(\mathbf{x} + \alpha \boldsymbol{\nu}) - \mathbf{F}(\mathbf{x} - \alpha \boldsymbol{\nu}) \right) \quad \mathbf{x} \in \Sigma.$$

We also fix the notation

$$\mathbf{F}^+ := \lim_{\alpha \searrow 0} \mathbf{F}(\mathbf{x} + \alpha \boldsymbol{\nu}), \quad \mathbf{F}^- := \lim_{\alpha \searrow 0} \mathbf{F}(\mathbf{x} - \alpha \boldsymbol{\nu}), \quad \text{for } \mathbf{x} \in \Sigma.$$

Next we introduce a convenient rescaling of the system to dimensionless form by setting the characteristic wavenumber of the ambient space to 1 [24]:

$$\begin{aligned} \mathbf{x} &\rightarrow \check{\mathbf{x}} = k_0 \mathbf{x}, & \nabla_s &\rightarrow \check{\nabla}_s = \frac{1}{k_0} \nabla_s, \\ \mu &\rightarrow \mu_r = \frac{1}{\mu_0} \mu, & \varepsilon &\rightarrow \varepsilon_r = \frac{1}{\varepsilon_0} \varepsilon, & \sigma^\Sigma &\rightarrow \sigma_r^\Sigma = \sqrt{\frac{\mu_0}{\varepsilon_0}} \sigma^\Sigma \\ \mathbf{E} &\rightarrow \check{\mathbf{E}} = \frac{k_0^2}{\omega \mu_0} \mathbf{E}, & \mathbf{H} &\rightarrow \check{\mathbf{H}} = k_0 \mathbf{H}, & k_z &\rightarrow \check{k}_z = \frac{k_z}{k_0}. \end{aligned}$$

To lighten the notation, we omit the breve sign in the remainder of this paper. Applying the rescaling to (2) and rewriting into tangential and normal parts leads to the following interface conditions:

$$(3) \quad \left\{ \begin{array}{l} [\mathbf{H}_s]_\Sigma \cdot \boldsymbol{\tau} = \left[\frac{i}{k_s^2} (k_z \partial_\tau H_z + \varepsilon_r \partial_\nu E_z) \right]_\Sigma = \sigma_r^\Sigma E_z, \\ [H_z]_\Sigma = -\sigma_r^\Sigma \mathbf{E}_s \cdot \boldsymbol{\tau}, \\ [\mu_r \mathbf{H}_s]_\Sigma \cdot \boldsymbol{\nu} = \left[\frac{i \mu_r}{k_s^2} (k_z \partial_\nu H_z - \varepsilon_r \partial_\tau E_z) \right]_\Sigma = 0, \\ [\mathbf{E}_s]_\Sigma \cdot \boldsymbol{\tau} = \left[\frac{i}{k_s^2} (k_z \partial_\tau E_z - \mu_r \partial_\nu H_z) \right]_\Sigma = 0, \\ [E_z]_\Sigma = 0, \\ [\varepsilon_r \mathbf{E}_s]_\Sigma \cdot \boldsymbol{\nu} = \left[\frac{i \varepsilon_r}{k_s^2} (k_z \partial_\nu E_z + \mu_r \partial_\tau H_z) \right]_\Sigma = \frac{1}{i} \nabla_s \cdot (\sigma_r^\Sigma \mathbf{E}_s), \end{array} \right.$$

where ∂_τ and ∂_ν denote the derivative in the tangential and the normal direction, respectively; $k_s(x, y)^2 = \mu_r(x, y) \varepsilon_r(x, y) - k_z^2$ is a function in the transverse direction; and where we have used the identities (see Appendix Appendix A)

$$(4) \quad \left\{ \begin{array}{l} k_s^2 \mathbf{E}_s = i (k_z \nabla_s E_z + \mu_r \nabla_s \times H_z), \\ k_s^2 \mathbf{H}_s = i (k_z \nabla_s H_z - \varepsilon_r \nabla_s \times E_z). \end{array} \right.$$

The first-order system (1) can be manipulated in a similar fashion (see Appendix Appendix A) to obtain

$$(5) \quad \left\{ \begin{array}{l} \nabla_s \times (\mu_r^{-1} \nabla_s \times \hat{z} E_z) + i k_z \nabla_s \times (\mu_r^{-1} \hat{z} \times \mathbf{E}_s) - \varepsilon_r E_z = 0, \\ \nabla_s \times (\varepsilon_r^{-1} \nabla_s \times \hat{z} H_z) + i k_z \nabla_s \times (\varepsilon_r^{-1} \hat{z} \times \mathbf{H}_s) + \mu_r H_z = 0. \end{array} \right.$$

2.2. Variational Statement

Let $\Omega \subset \mathbb{R}^n$, where $n = 2, 3$, be a simply connected and bounded domain with Lipschitz-continuous piecewise smooth boundary, $\partial\Omega$. Assume, in addition, that Σ is a Lipschitz-continuous, piecewise smooth hypersurface. Let $\boldsymbol{\nu}$ and $\boldsymbol{\tau}$ denote the outer normal and the tangential vector on Σ (see Figure 2). Some algebraic manipulation shows that $\nabla_s \times (\mu_r^{-1} \nabla_s \times \hat{z} E_z) = -\nabla_s \cdot (\mu_r^{-1} \nabla_s \hat{z} E_z)$ and $\nabla_s \times (\mu_r^{-1} \hat{z} \times \mathbf{E}_s) = \hat{z} \nabla_s \cdot (\mu_r^{-1} \mathbf{E}_s)$, which can be used in conjunction with (A.5) and (5) to obtain:

$$(6) \quad \begin{cases} -\nabla_s \cdot \left(\frac{\varepsilon_r}{k_s^2} \nabla_s E_z \right) - k_z \nabla_s \cdot \left(\frac{1}{k_s^2} \nabla_s \times \hat{z} H_z \right) - \varepsilon_r E_z = 0, \\ -\nabla_s \cdot \left(\frac{\mu_r}{k_s^2} \nabla_s H_z \right) + k_z \nabla_s \cdot \left(\frac{1}{k_s^2} \nabla_s \times \hat{z} E_z \right) - \mu_r H_z = 0. \end{cases}$$

We observe that if the domain is homogeneously filled and isotropic, the curl terms vanish, yielding the familiar decoupled Helmholtz equation for E_z and H_z . Now assume that

$$(7) \quad [\varepsilon_r]_\Sigma = 0, \quad [\mu_r]_\Sigma = 0.$$

For the sake of brevity, we summarize the derivation here and refer the reader to Appendix Appendix A for details. By multiplying (6) by k_s^4 and testing the first equation by φ and the second equation by ψ , we obtain

$$(8) \quad \begin{aligned} & (\mu_r \varepsilon_r^2 \nabla_s E_z, \nabla_s \varphi) + 2(\varepsilon_r \nabla_s E_z, \nabla_s (\bar{\varepsilon}_r \bar{\mu}_r) \varphi) \\ & + k_z (\mu_r \varepsilon_r \nabla_s \times \hat{z} H_z, \nabla_s \varphi) - k_z^2 (\varepsilon_r \nabla_s E_z, \nabla_s \varphi) \\ & + 2k_z (\nabla_s \times \hat{z} H_z, \nabla_s (\bar{\varepsilon}_r \bar{\mu}_r) \varphi) - k_z^3 (\nabla_s \times \hat{z} H_z, \nabla_s \varphi) - (\varepsilon_r k_s^4 E_z, \varphi) \\ & + (\varepsilon_r \mu_r^2 \nabla_s H_z, \nabla_s \psi) + 2(\mu_r \nabla_s H_z, \nabla_s (\bar{\varepsilon}_r \bar{\mu}_r) \psi) \\ & - k_z (\mu_r \varepsilon_r \nabla_s \times \hat{z} E_z, \nabla_s \psi) - k_z^2 (\mu_r \nabla_s H_z, \nabla_s \psi) \\ & - 2k_z (\nabla_s \times \hat{z} E_z, \nabla_s (\bar{\varepsilon}_r \bar{\mu}_r) \psi) + k_z^3 (\nabla_s \times \hat{z} E_z, \nabla_s \psi) - (\mu_r k_s^4 H_z, \psi) \\ & - i \langle \sigma_r^\Sigma k_s^4 E_z, \varphi \rangle_\Sigma = 0. \end{aligned}$$

This shows the following statement.

Proposition 1. *Provided that $k_s \neq 0$ and $[\varepsilon_r]_\Sigma = [\mu_r]_\Sigma = 0$, the nonlinear eigenvalue problem*

$$(N) \quad \text{Find } k_z \in \mathbb{C} \setminus \{0\} \text{ and } E_z, H_z \text{ s. t. (6) and (3) are satisfied}$$

can be restated as a quartic eigenvalue problem

(Q)

Find $k_z \in \mathbb{C} \setminus \{0\}$ and $E_z, H_z \in \mathbf{X}(\Omega) = \{(u, v) : u, v \in H^1(\Omega, \mathbb{C})\}$ s. t.

$$\mathcal{Q}(k_z, (E_z, H_z))[(\varphi, \psi)] = 0 \quad \text{for all } \varphi, \psi \in H^1(\Omega, \mathbb{C}),$$

where

$$\mathcal{Q}(k_z, (E_z, H_z))[(\varphi, \psi)] = \sum_{l=0}^4 (k_z)^l a_l((E_z, H_z))[(\varphi, \psi)],$$

and

(9)

$$\left\{ \begin{array}{l} a_0((E_z, H_z), (\varphi, \psi)) = (\mu_r \varepsilon_r^2 \nabla_s E_z, \nabla_s \varphi) + 2(\varepsilon_r \nabla_s E_z, (\nabla_s \bar{\mu}_r \bar{\varepsilon}_r) \varphi) \\ \quad - (\mu_r^2 \varepsilon_r^3 E_z, \varphi) + (\varepsilon_r \mu_r^2 \nabla_s H_z, \nabla_s \psi) \\ \quad + 2(\mu_r \nabla_s H_z, (\nabla_s \bar{\mu}_r \bar{\varepsilon}_r) \psi) \\ \quad - (\mu_r^3 \varepsilon_r^2 H_z, \psi) - i \langle \sigma_r^\Sigma \mu_r^2 \varepsilon_r^2 E_z, \varphi \rangle_\Sigma, \\ a_1((E_z, H_z), (\varphi, \psi)) = (\mu_r \varepsilon_r \nabla_s \times \hat{z} H_z, \nabla_s \varphi) \\ \quad + 2(\nabla_s \times \hat{z} H_z, (\nabla_s \bar{\mu}_r \bar{\varepsilon}_r) \varphi) \\ \quad - (\mu_r \varepsilon_r \nabla_s \times \hat{z} E_z, \nabla_s \psi) \\ \quad - 2(\nabla_s \times \hat{z} E_z, (\nabla_s \bar{\mu}_r \bar{\varepsilon}_r) \psi) \\ a_2((E_z, H_z), (\varphi, \psi)) = -(\varepsilon_r \nabla_s E_z, \nabla_s \varphi) + 2(\mu_r \varepsilon_r^2 E_z, \varphi) \\ \quad - (\mu_r \nabla_s H_z, \nabla_s \psi) + 2(\mu_r^2 \varepsilon_r H_z, \psi) \\ \quad + 2i \langle \sigma_r^\Sigma \mu_r \varepsilon_r E_z, \varphi \rangle_\Sigma, \\ a_3((E_z, H_z), (\varphi, \psi)) = -(\nabla_s \times \hat{z} H_z, \nabla_s \varphi) + (\nabla_s \times \hat{z} E_z, \nabla_s \psi), \\ a_4((E_z, H_z), (\varphi, \psi)) = -(\varepsilon_r E_z, \varphi) - (H_z, \psi) - i \langle \sigma_r^\Sigma E_z, \varphi \rangle_\Sigma. \end{array} \right.$$

3. Numerical approach

In this section, we outline our numerical approach for solving the quartic eigenvalue problem (Q). In particular we discuss a *quadratisation* approach transforming the quartic eigenvalue problem into a larger, linear eigenvalue problem with equivalent spectrum. A perfectly matched layer (PML), an artificial sponge layer placed near the boundary such that all outgoing waves

decay exponentially, is introduced. The variational formulation (Q) is discretized on a non-uniform quadrilateral mesh.

Proposition 2. *Let $\mathbf{X}_h(\Omega) \subset \mathbf{X}(\Omega)$ be a finite element subspace spanned by Lagrange finite elements Q_p .*

$$(Q_h) \quad \sum_{l=0}^4 k_z^l a_l((E_z, H_z), (\varphi, \psi)) = 0,$$

Our goal is to translate (Q_h) into a finite dimensional linear problem, which then allows the use of a standard linear algebra solver.

3.1. Quadratication of the Quartic Eigenvalue Problem

We build upon the algebraic tool of *quadratication* introduced in [13], which allows us to reduce any even power matrix polynomial eigenvalue problem to a spectrally equivalent linear eigenvalue problem. Prop. 3 summarizes the main result (for a more general discussion of the ideas behind this reduction procedure, we refer the reader to [13]).

Proposition 3 (Theorem 5.3 and 5.4 of [13]). *Consider a quartic eigenvalue problem, to find $\lambda \in \mathbb{C}$, and $x \in \mathbb{C}^n$, s. t.*

$$\sum_{k=0}^4 \lambda^k A_k x = 0,$$

where $A_k \in \mathbb{C}^{n \times n}$ are given matrices. Then, the linearization stated below is spectrally equivalent to the original problem (c.f. [13] Theorem 5.3 and 5.4): Find $\lambda \in \mathbb{C}$, and $z \in \mathbb{C}^{4n}$ s. t.

$$(10) \quad \begin{pmatrix} A_3 & 0 & -I_n & 0 \\ A_1 & 0 & 0 & -I_n \\ 0 & -I_n & 0 & 0 \\ A_0 & 0 & 0 & 0 \end{pmatrix} z + \lambda \begin{pmatrix} A_4 & 0 & 0 & 0 \\ A_2 & I_n & 0 & 0 \\ 0 & 0 & I_n & 0 \\ 0 & 0 & 0 & I_n \end{pmatrix} z = 0.$$

Here, I_n denotes the $n \times n$ identity matrix.

With this result at hand, we rewrite (Q_h) as a linear eigenvalue problem:

$$(LQ_h) \quad S z + \lambda M z = 0,$$

where

$$S = \begin{pmatrix} a_3 & 0 & -I_n & 0 \\ a_1 & 0 & 0 & -I_n \\ 0 & -I_n & 0 & 0 \\ a_0 & 0 & 0 & 0 \end{pmatrix}, \quad M = \begin{pmatrix} a_4 & 0 & 0 & 0 \\ a_2 & I & 0 & 0 \\ 0 & 0 & I & 0 \\ 0 & 0 & 0 & I \end{pmatrix}, \quad z = \begin{pmatrix} z_1 \\ z_2 \\ z_3 \\ z_4 \end{pmatrix}.$$

Here, by some abuse of notation a_i denotes the corresponding matrix formed by the bilinear form $a_i(\cdot, \cdot)$ given in (9) and by fixing a basis of $\mathbf{X}_h(\Omega)$. A quick computation shows that the eigenvectors of the original problem (Q_h) and of the final linearized problem (LQ_h) are related as follows.

Proposition 4. *Let $\lambda \in \mathbb{C}$ and $x \in \mathbb{C}^n$ be an eigenvalue with corresponding eigenvector of (Q_h) . Then, λ and $z \in \mathbb{C}^{4n}$ given by*

$$(11) \quad \begin{cases} z_1 &= \lambda x, \\ z_2 &= \lambda^2(a_3 + \lambda a_4)x, \\ z_3 &= \lambda(a_3 + \lambda a_4)x, \\ z_4 &= -a_0 x, \end{cases}$$

is an eigenvalue with corresponding eigenvector of (LQ_h) . Conversely, if $\lambda \in \mathbb{C}$ and $z \in \mathbb{C}^{4n}$ is an eigenvalue and eigenvector pair of (LQ_h) , then provided that $\det(a_0) \neq 0$ and $\det(\lambda a_4 + a_3) \neq 0$, the vector z is characterized by (11) and λ and x are an eigenvalue and eigenvector pair of (Q_h) .

3.2. Perfectly Matched Layer

A perfectly matched layer (PML) is a truncation procedure motivated from electromagnetic scattering problems in the time domain. The idea is to surround the computational domain with a so-called sponge layer, an artificial boundary wherein all outgoing electromagnetic waves decay exponentially with minimal artificial reflection. As outlined in [25, 26, 24], we carry out a change of coordinates from the computational domain with real-valued coordinates to a domain with complex-valued coordinates. We refer the reader to [25] for details. For a spherical absorption layer, we define the transformation $\tilde{\rho} = \rho \bar{d}$, where

$$d = 1 + is(r), \quad \bar{d} = 1 + i/r \int_{\rho}^r s(\tau) d\tau,$$

and $s(\tau)$ is an appropriately chosen, nonnegative scaling function. Applying the above transformation, the quartic eigenvalue problem takes the following

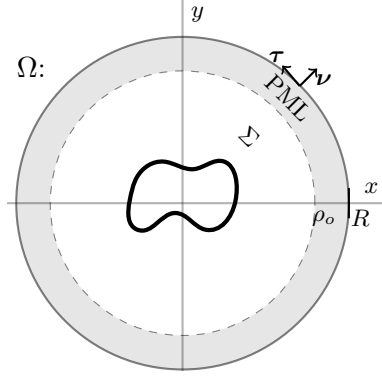


Figure 2: Schematic of the computational domain of a circular waveguide Ω , with boundary $\partial\Omega$, outer normal vector $\boldsymbol{\nu}$, and tangential vector $\boldsymbol{\tau}$. A conducting circular interface is labeled Σ . A perfectly matched layer (PML) is enforced in the shaded region.

rescaled form within the PML:

$$\begin{aligned}
& \hat{\nabla}_s \cdot (k_s^2 (\varepsilon_r \hat{\nabla}_s \hat{E}_z)) - 2k_s^2 \hat{\nabla}_s \cdot (\varepsilon_r \hat{\nabla}_s \hat{E}_z) + k_z \hat{\nabla}_s \cdot (k_s^2 \hat{\nabla}_s \times \hat{H}_z) \\
& - 2k_z k_s^2 \hat{\nabla}_s \cdot (\hat{\nabla}_s \times \hat{H}_z) + \hat{\nabla}_s \cdot (k_s^2 (\mu_r \hat{\nabla}_s \hat{H}_z)) - 2k_s^2 \hat{\nabla}_s \cdot (\mu_r \hat{\nabla}_s \hat{H}_z) \\
& + k_z \hat{\nabla}_s \cdot (k_s^2 \hat{\nabla}_s \times \hat{E}_z) + 2k_z k_s^2 \hat{\nabla}_s \cdot (\hat{\nabla}_s \times \hat{E}_z) \\
& - \varepsilon_r k_s^4 \hat{E}_z - \mu_r k_s^4 \hat{H}_z = 0.
\end{aligned}$$

This can be rewritten as

$$\begin{aligned}
& \frac{1}{d\bar{d}} \nabla_s \cdot (k_s^2 \varepsilon_r A \nabla_s E_z) - \frac{2k_s^2}{d\bar{d}} \nabla_s \cdot (\varepsilon_r A \nabla_s E_z) + \frac{k_z}{d\bar{d}} \nabla_s \cdot (k_s^2 \nabla_s \times H_z) \\
& - \frac{2k_z k_s^2}{d\bar{d}} \nabla_s \cdot (\nabla_s \times H_z) + \frac{1}{d\bar{d}} \nabla_s \cdot (k_s^2 \varepsilon_r A \nabla_s E_z) - \frac{2k_s^2}{d\bar{d}} \nabla_s \cdot (\varepsilon_r A \nabla_s E_z) \\
& + \frac{k_z}{d\bar{d}} \nabla_s \cdot (k_s^2 \nabla_s \times H_z) + \frac{2k_z k_s^2}{d\bar{d}} \nabla_s \cdot (\nabla_s \times E_z) \\
& + \varepsilon_r k_s^4 E_z + \mu_r k_s^4 H_z = 0,
\end{aligned}$$

where $A = T_{\mathbf{e}_x, \mathbf{e}_r}^{-1} \text{diag}(\bar{d}/d, d/\bar{d}) T_{\mathbf{e}_x, \mathbf{e}_r}$, and $T_{\mathbf{e}_x, \mathbf{e}_r}$ is the rotation matrix that rotates \mathbf{e}_r onto \mathbf{e}_x . We enforce the condition that the material parameters are constant outside the PML, i.e., ε_r and μ_r do not undergo a change of coordinate. Additionally, because the eigenmodes of our interest are confined to the conducting interface, which is situated inside the PML, no coordinate change is needed for the jump condition. The modified bilinear forms, \tilde{a}_i ,

are

$$(12) \quad \left\{ \begin{array}{l} \tilde{a}_0((E_z, H_z), (\varphi, \psi)) = (\varepsilon_r^2 A \nabla_s E_z, \nabla_s \varphi) + 2(\varepsilon_r A \nabla_s E_z, (\nabla_s \bar{\varepsilon}_r) \varphi) \\ \quad - d\bar{d}(\varepsilon_r^3 E_z, \varphi) + (\varepsilon_r A \nabla_s H_z, \nabla_s \psi) \\ \quad + 2(A \nabla_s H_z, (\nabla_s \bar{\varepsilon}_r) \psi) - d\bar{d}(\varepsilon_r^2 H_z, \psi) \\ \quad - i\langle \sigma_r^\Sigma \varepsilon_r^2 E_z, \varphi \rangle_\Sigma, \\ \tilde{a}_1((E_z, H_z), (\varphi, \psi)) = (\varepsilon_r \nabla_s \times \hat{z} H_z, \nabla_s \varphi) \\ \quad + 2(\nabla_s \times \hat{z} H_z, (\nabla_s \bar{\varepsilon}_r) \varphi) \\ \quad - (\varepsilon_r \nabla_s \times \hat{z} E_z, \nabla_s \psi) \\ \quad - 2(\nabla_s \times \hat{z} E_z, (\nabla_s \bar{\varepsilon}_r) \psi) \\ \tilde{a}_2((E_z, H_z), (\varphi, \psi)) = -(\varepsilon_r A \nabla_s E_z, \nabla_s \varphi) + 2d\bar{d}(\varepsilon_r^2 E_z, \varphi) \\ \quad - (A \nabla_s H_z, \nabla_s \psi) + 2d\bar{d}(\varepsilon_r H_z, \psi) \\ \quad + 2i\langle \sigma_r^\Sigma \varepsilon_r E_z, \varphi \rangle_\Sigma, \\ \tilde{a}_3((E_z, H_z), (\varphi, \psi)) = -(\nabla_s \times \hat{z} H_z, \nabla_s \varphi) + (\nabla_s \times \hat{z} E_z, \nabla_s \psi), \\ \tilde{a}_4((E_z, H_z), (\varphi, \psi)) = -d\bar{d}(\varepsilon_r E_z, \varphi) - d\bar{d}(H_z, \psi) - i\langle \sigma_r^\Sigma E_z, \varphi \rangle_\Sigma. \end{array} \right.$$

3.3. Möbius Transform

The Möbius transformation is an efficient tool that transforms the given eigenvalue problem into a related one, for which eigenvalues of interest in the transformed spectrum are close to 0 (or maximal), so that they can be selectively computed with conventional Krylov-space iteration techniques. It is a conformal mapping, defined as follows.

$$\lambda \mapsto \frac{a\lambda + b}{c\lambda + d},$$

where $\lambda, a, b, c, d \in \mathbb{C}$. Over arbitrary fields, the Möbius transformation preserves a number of spectral features of matrix polynomials, such as regularity, rank, minimal indices, the location of zero entries, symmetry, and skew-symmetry [27]. In particular, every Möbius transformation preserves the relation of spectral equivalence [27]. The computational eigenvalue problem, after introducing a PML, truncating the domain, and applying finite elements, can be written as

$$(13) \quad Sz = k_z Mz,$$

	Eigenvalues from (L)	Eigenvalues from (Q)	Eigenvalues from (18)
Mode	k_z	k_z	k_z
1	$9.447 \pm 0.090468i$	$9.447 \pm 0.090467i$	$9.447 \pm 0.090467i$
2	$13.00 \pm 0.090641i$	$13.00 \pm 0.090640i$	$13.00 \pm 0.090641i$
3	$16.17 \pm 0.099812i$	$16.17 \pm 0.099812i$	$16.17 \pm 0.099813i$

Table 1: Validation of computed eigenvalues from the linear problem (15), the quartic problem (Q), and the analytical approach (18) for a single-layer waveguide. Note that the values obtained are in agreement with confidence level of less than 1%. Parameters used are $R = 2.0$, $\sigma_r^\Sigma = 0.002 + 0.20i$, $\varepsilon_r = \mu_r \equiv 1$, and $\rho_i = 0.3$.

for a complex-valued vector z and appropriate complex-valued matrices S and M . The implementation of the PML discussed in 3.2 necessitates changes to the definition of a_1, a_2, a_3 , and a_4 . The idea is to use the Möbius transform to map points near the origin to target values

$$(14) \quad (aS + bM)z = \tilde{k}_z(cS + dM)z,$$

where a, b, c, d are the Möbius transform parameters. The original eigenvalue can be retrieved via the inverse Möbius transform $k_z = (-b + d\tilde{k}_z)/(a - c\tilde{k}_z)$.

4. Validation of weak formulation

In this section, the analytical solution for constant material parameters is derived and discussed. We use the analytic result to validate our numerical approach.

By assuming constant material parameters, the quartic eigenvalue problem (Q) does not exhibit any hybridization and reduces to a linear eigenvalue problem: Find $u \in H^1(\Omega, \mathbb{C})$ s. t.

$$(L) \quad \mathcal{L}(u)[\varphi] := a(u, \varphi) + k_z^2 m(u, \varphi),$$

for $\varphi \in H^1(\Omega, \mathbb{C})$ and where we have introduced the bilinear forms

$$(15) \quad \begin{cases} a(u, \varphi) = \int_{\Omega} \nabla_s u \cdot \nabla_s \bar{\varphi} \, dx - \int_{\Omega} \mu_r \varepsilon_r u \bar{\varphi} \, dx - i \int_{\Sigma} \mu_r \sigma_r^\Sigma u \bar{\varphi} \, do_x, \\ m(u, \varphi) = \int_{\Omega} u \bar{\varphi} \, dx + i \int_{\Sigma} \sigma_r^\Sigma \varepsilon_r^{-1} u \bar{\varphi} \, do_x. \end{cases}$$

For a simple spherical geometry that is rotationally invariant, the field solution can be expressed as a superposition of the modified Bessel functions of the first and second kind. In the case of a waveguide with a single circular

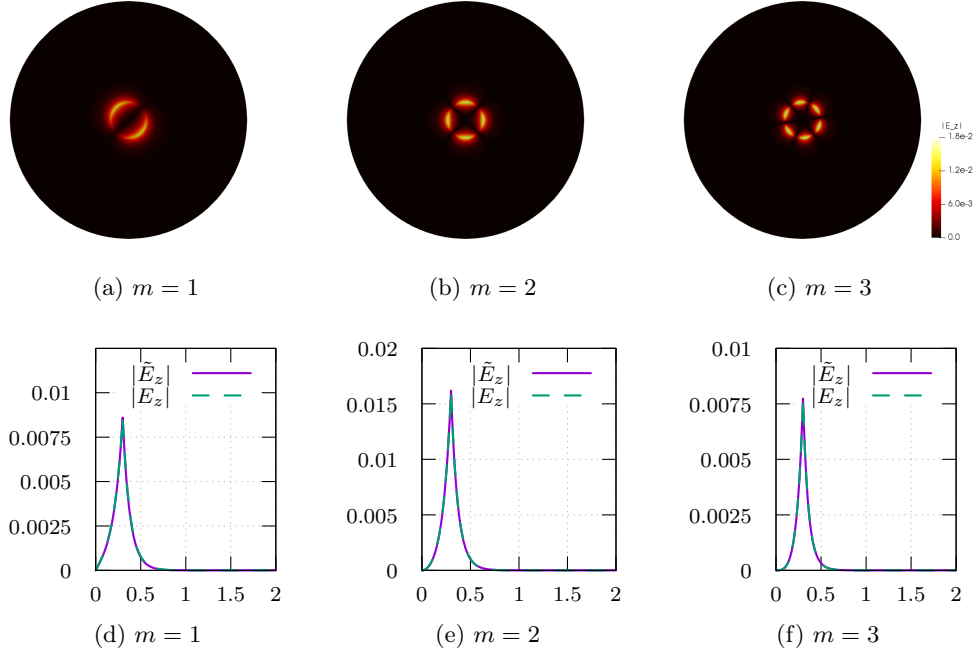


Figure 3: Computational results for modal order $m = 1, 2, 3$ for a spherical reference configuration with constant material parameters, with interior radius $\rho_i = 0.3$, $\sigma_r^\Sigma = 0.002 + 0.20i$, and $R = 2.0$. (a-c) shows the magnitude of the numerically computed electric field, \tilde{E}_z . The computed electric field is compared against an analytic solution, E_z , in (d)-(f).

interface Σ , i.e., where Σ is described by a circle with origin 0 and radius R , the analytical solution takes the following form.

$$(16) \quad E_z = \begin{cases} A_m I_m(ik_s \rho) e^{im\theta} e^{ik_z z} & \text{for } \rho < R, \\ B_m K_m(ik_s \rho) e^{im\theta} e^{ik_z z} & \text{for } \rho > R, \end{cases}$$

$$(17) \quad H_z = \begin{cases} C_m I_m(ik_s \rho) e^{im\theta} e^{ik_z z} & \text{for } \rho < R, \\ D_m K_m(ik_s \rho) e^{im\theta} e^{ik_z z} & \text{for } \rho > R, \end{cases}$$

where I_m and K_m denote the modified Bessel functions of the first and second kind, respectively, and A_m, B_m, C_m , and D_m are constants that are determined by the boundary conditions [15, 3]. Assuming that the conducting film is located on the boundary of the interior circle with radius R , we equate the jump conditions (3) of each field component. Then (3) reduces to the following algebraic condition, from which we can retrieve the propagation

constant, k_z :

$$(18) \quad \det(M - \sigma_r^\Sigma N) = 0,$$

where

$$M := \begin{pmatrix} I_m(ik_s R) & 0 & -K_m(ik_s R) & 0 \\ \frac{k_z m I_m(ik_s R)}{R k_s^2} & -\frac{\mu I'_m(ik_s R)}{k_s} & -\frac{k_z m K_m(ik_s R)}{R k_s^2} & \frac{\mu K'_m(ik_s R)}{k_s} \\ \frac{\epsilon_1 I'_m(ik_s R)}{k_s} & \frac{k_z m I_m(ik_s R)}{R k_s^2} & -\frac{\epsilon_2 K'_m(ik_s R)}{k_s} & -\frac{k_z m K_m(ik_s R)}{R k_s^2} \\ 0 & I_m(ik_s R) & 0 & -K_m(ik_s R) \end{pmatrix}$$

and

$$N := \begin{pmatrix} 0 & 0 & 0 & 0 \\ 0 & 0 & 0 & 0 \\ I_m(ik_s R) & 0 & 0 & 0 \\ -\frac{k_z m I_m(ik_s R)}{R k_s^2} & \frac{\mu I'_m(ik_s R)}{k_s} & 0 & 0 \end{pmatrix}.$$

We numerically solve the zeroes of the determinant of the difference of the above matrices via a root finding algorithm for modal orders $m = 1, 2$ and 3 . The computed values are then compared against those of the linear problem (L) and of the quartic problem (Q) (see Table 1 and Figure 3).

We now validate our numerics with the analytical results. Three validations are carried out: analytical, numerical with linear eigenvalue, and lastly, the quartic eigenvalue problem. For simplicity, we assume the computational domain is isotropic, with material parameters $\epsilon_r = \mu_r \equiv 1$. A conducting interface is coated on the boundary of the interior circle with radius $\rho_i = 0.3$, and choose $R = 2.0$. The surface conductivity is set to $\sigma_r^\Sigma = 0.002 + 0.20i$.

The analytic computation of the propagation constant k_z requires finding the complex roots of the determinant of the 4×4 matrix. We will consider modal orders of $m = 1, 2$ and 3 to ease the computation. The computational results displayed in Table 1 deviate by less than 1% from each other. We can thus expect a confidence level of 1% or better in our numerical computations. Figure 3 shows the intensity of the numerically computed electric field, $\|E_z\|_2$, and a comparison of, both, the analytic and numerical solutions. We thus conclude that our numerical framework is a reliable model that can effectively simulate hybrid plasmonic modes.

5. Numerical results

These eigenvalues are numerically computed using SLEPc [12], a general purpose eigensolver built on top of PETSc [11]. The eigensolver provides a number of Krylov-space methods, such as the Arnoldi, Lanczos, Krylov-Schur, and conjugate-gradient methods. For our purposes, we will make use of the Krylov-Schur method for its faster convergence.

In this section, we present a number of computational results obtained from solving the quartic eigenvalue problem (Q). We examine numerically how the spectrum of a hybridized configuration behaves under modification of spatially dependent material parameters, $\varepsilon_r(\rho, \theta)$. We further investigate the relationship between mesh deformation and a quality factor, and study the degree by which the spectrum changes. All numerical computations are carried out with the finite element library deal.II [10]. We use a Krylov-Schur method to compute solutions of the linearized eigenproblem (LQ_h) [12].

We demonstrate numerically how it is possible to attain an improved quality factor by prescribing the host material with a radially-varying refractive index profile. This is methodically carried out in the subsequent subsections. First, a parameter study is conducted to validate our choice of discretization parameters. Second, we solve the quartic eigenvalue problem (LQ_h) using a number of permittivity functions, and observe how the spectrums differ from those obtained in an isotropic medium. Lastly, we deform our computational domain to demonstrate that our numerical framework is equipped to handle even the most general configuration. The key idea behind this generalization is to show that we can manipulate the spectrum by manipulating the shape. We make note of the evolution of eigenmodes, and how our framework can be used as a basis for shape optimization of gradient-index waveguides.

5.1. Validation of discretization parameters

The computational domain, Ω , is chosen to be the circle with radius 1. A spherical PML is enforced for $\rho > 0.8$. The surface conductivity $\sigma_r^\Sigma = 0.002 + 0.20i$ is chosen that is within a realistic parameter range [24]. Following [26], the nonnegative scaling function $s(\rho)$ is chosen to be

$$(19) \quad s(\rho) = s_0 \frac{(\rho - 0.8R)^2}{(R - 0.8R)^2},$$

where we set the free parameter s_0 to be $s_0 = 1.5$ in our computations. We carry out a parameter study to test the validity and the sensitivity of

	$s_o = 1.5, R = 1.0, k = 4, \text{DoF} = 19138$			$s_o = 1.5, R = 1.0, k = 6, \text{DoF} = 303874$		
Mode	$\text{Re}k_z$	$\text{Im}k_z$	$\text{Re}k_z/\text{Im}k_z$	$\text{Re}k_z$	$\text{Im}k_z$	$\text{Re}k_z/\text{Im}k_z$
1	30.5400	0.17646	173.070	30.4160	0.17540	173.409
2	40.5520	0.21898	185.186	40.5043	0.21881	185.112

(a) Vary the number of refinements, k .

	$s_o = 1.5, R = 1.0, k = 5, \text{DoF} = 76162$		
Mode	$\text{Re}k_z$	$\text{Im}k_z$	$\text{Re}k_z/\text{Im}k_z$
1	30.4160	0.17582	172.995
2	40.5043	0.21881	185.112

(b) The control case for the parameter studies.

	$s_o = 1.5, R = 0.5, k = 5, \text{DoF} = 76162$			$s_o = 1.5, R = 2.0, k = 5, \text{DoF} = 76162$		
Mode	$\text{Re}k_z$	$\text{Im}k_z$	$\text{Re}k_z/\text{Im}k_z$	$\text{Re}k_z$	$\text{Im}k_z$	$\text{Re}k_z/\text{Im}k_z$
1	30.4242	0.17528	173.575	30.8567	0.17331	178.043
2	40.4905	0.21876	185.091	40.5043	0.21881	185.112

(c) Vary the domain size, R .

Table 2: Parameter study with permittivity function $\varepsilon_r(\mathbf{x}) = 3 \cdot \chi_{|\mathbf{x}| < \rho_i} + 1 \cdot \chi_{\rho_i < |\mathbf{x}| < R}$. $\mu_r(\mathbf{x}) \equiv 1$ and $\sigma_r^\Sigma = 0.002 + 0.20i$. (b) is the control discretization parameters. (a) differs from (b) in the number of refinements, and (c) differs from (b) in the size of the domain.

discretization parameters. Table 2 summarizes the parameter study quantitatively. As can be seen, the eigenmodes computed are stable with respect to variations of PML strength s_0 , the number of initial refinements k , and domain sizes R . A spectral transformation is carried out in the form of the Möbius transformation, with the parameters chosen to be $a = 1, b = -10, c = 1, d = 10$. We conclude that $R = 1.0$ and $k = 5$ is a valid choice of discretization parameters.

5.2. Gradient-index waveguide

Our numerical framework admits any (locally) differentiable material parameters. To demonstrate this, we consider the following material permittivity functions and analyze their spectrums in relation to those of the isotropic

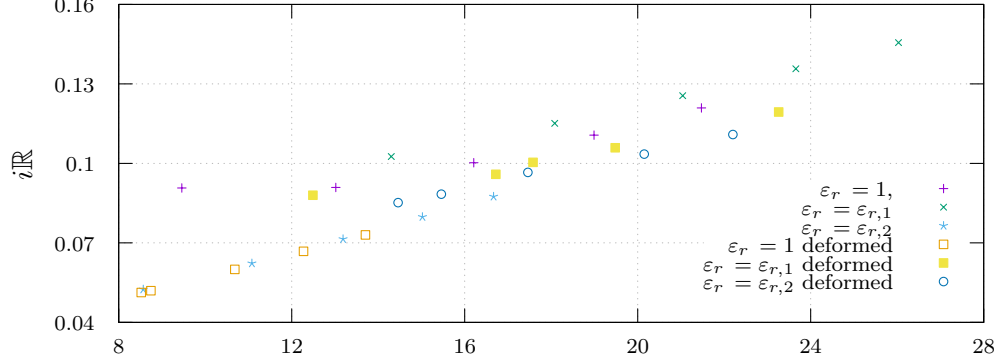


Figure 4: Spectrums computed using different $\epsilon \mathbb{R}$ for spherical and deformed domain. For $\epsilon_r \equiv 1$ and $\epsilon_{r,1}$, both the real and the imaginary parts have decreased after the domain was deformed. The opposite is observed for $\epsilon_{r,2}$. In the spherical domain case, the eigenvalues for $\epsilon_r \equiv 1$ and $\epsilon_{r,1}$ remain relatively close to one another, but undergo a noticeable difference after the mesh deformation. The opposite can be seen for $\epsilon_{r,1}$ and $\epsilon_{r,2}$.

medium.

$$(20) \quad \begin{cases} \epsilon_{r,1}(\rho, \theta) = 1.2 + \frac{1}{2} \sin\left(\frac{\rho^2}{(2\rho_i)^2} \sin 2\theta\right) \exp\left(-\frac{(\rho - 2\rho_i)^2}{(2\rho_i)^2}\right), \\ \epsilon_{r,2}(\rho) = 1 + \left(\frac{\rho}{2} + \rho^2 \sin\left(\frac{2\pi}{\rho}\right)\right) \exp\left(-\frac{(\rho - 2\rho_i)^2}{2\rho_i}\right), \end{cases}$$

where ρ_o is the PML cutoff radius and ρ_i is the radius at which the conducting interface is situated for a circular waveguide. We set $\rho_o = 0.8$ and $\rho_i = 0.1$ for our computations. The key aspect of these functions is that ϵ_r remains constant in the PML, which enables us to implement the PML as laid out in 3.2. The computations are carried out using the unit circular waveguide. For comparison, we plot the eigenvalues for both isotropic media and materials defined by (20) (see Figure 4). The quality factor of the first 5 modes of each of these functions are laid out in Table 3. We make note of a few observations.

- The eigenvalues obtained from $\epsilon_{r,i}$ are more clustered than those from isotropic media. Even though the range of $\epsilon_{r,i}$ ($\epsilon_{r,1} \in (1.0, 1.4)$ and $\epsilon_{r,2} \in (1.0, 1.1614)$) is relatively close to 1, we observe significant changes to the spectrum and the quality factor.
- From Table 3, a much longer propagation is observed for $\epsilon_{r,2}$ than for $\epsilon_{r,1}$, despite their relatively similar range.

Mode	$\varepsilon_r \equiv 1$			$\varepsilon_r = \varepsilon_{r,1}$			$\varepsilon_r = \varepsilon_{r,2}$		
	$\text{Re}k_z$	$\text{Im}k_z$	η_3	$\text{Re}k_z$	$\text{Im}k_z$	η	$\text{Re}k_z$	$\text{Im}k_z$	η
1	13.02	0.09093	143.2	14.30	0.1026	139.4	8.569	0.05243	163.4
2	16.21	0.1003	161.7	18.08	0.1151	157.1	11.08	0.06230	177.9
3	18.99	0.1107	171.6	21.04	0.1256	167.6	13.19	0.07144	184.6
4	21.47	0.1210	177.6	23.66	0.1357	174.3	15.02	0.07979	188.3
5	23.74	0.1309	181.4	26.03	0.1456	178.8	16.67	0.08746	190.6

(a) Eigenvalues for spherical domain

Mode	$\varepsilon_r \equiv 1$			$\varepsilon_r = \varepsilon_{r,1}$			$\varepsilon_r = \varepsilon_{r,2}$		
	$\text{Re}k_z$	$\text{Im}k_z$	η_3	$\text{Re}k_z$	$\text{Im}k_z$	η	$\text{Re}k_z$	$\text{Im}k_z$	η
1	8.521	0.05126	166.2	12.49	0.0880	141.9	14.46	0.0852	169.8
2	8.745	0.05194	168.8	16.72	0.0959	163.8	15.46	0.0884	174.9
3	10.69	0.06003	178.0	17.58	0.1004	175.1	17.46	0.0966	182.1
4	12.27	0.06683	183.7	19.48	0.1059	184.0	20.15	0.1035	194.8
5	13.71	0.07300	187.8	23.26	0.1194	194.8	22.20	0.1109	200.2

(b) Eigenvalues for deformed domain

Table 3: Eigenvalues k_z and quality factor η for different ε_r in spherical and deformed domains. Noticeable shift in the spectrums is observed from (a) to (b), which in turn, has led to non-negligible increases in η .

- This demonstrates that the relationship between ε_r and η is not trivial, and that it is possible to optimize η with a nontrivial ε_r .

5.3. Generalized configuration

Now, as a small study, we compute using the permittivity functions introduced in the preceding section, but in a deformed configuration, and demonstrate that we can use this generalization in the context for shape optimization. Meshes near the conducting interface are heavily deformed via the mapping $\delta = (\delta_x, \delta_y)$. The only restriction we impose is that the boundary of the computational domain is circular so as to preserve the spherical PML.

$$(21) \quad \begin{cases} \delta_x = 0.8x(1 - \arctan^2(4x)) \cdot (1 + \exp(-|x|)) \cdot \left(1 - \frac{|x|}{\sqrt{R^2 - y^2}}\right)^2, \\ \delta_y = \mp A \sin^2(\pi y^2/RT) \cdot (1 + \exp(\mp \rho_i y)) \cdot \left(1 - \frac{|y|}{\sqrt{R^2 - x^2}}\right)^2, \end{cases}$$

where A is the displacement amplitude, T is the displacement period, and ρ_i is the inner radius of the original mesh. For our purpose, we let $A = 55$

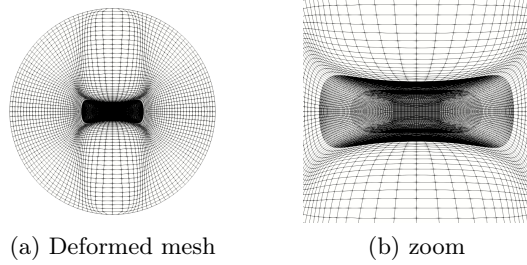


Figure 5: The deformed mesh (a) obtained with the mapping function δ outlined below. The mesh has a total number of around 370,000 cells. Additional refinements are a priori enforced around the conducting interface.

and $T = 15$. The resultant domain is shown in Figure 5 and numerical output can be found in Table 3(b). In Figure 6, we plot the magnitude of hybridized magnetic fields with modal order $m = 4$, with $\varepsilon_r = \varepsilon_{r,1}$ and $\varepsilon_{r,2}$. The conducting interface has been stretched, which induces a stronger plasmon interaction, and in turn, an improved quality factor. From Table 3, we observe that the spectrum can be manipulated by changing the geometry and that the relationship between the choice of ε_r and η is not trivial. This presents a potential future research topic for the designing of optical devices.

6. Conclusions and Outlook

In this paper, we formulated a variational framework for the numerical simulation of guided modes in a waveguide setting with gradient-index host. This resulted in a quartic eigenvalue problem, which was linearized via a quadratification approach. The eigenmodes of interest are electromagnetic SPPs that arise on a conducting closed curve, e.g., graphene-coated waveguide. The interface is modeled by an idealized, oriented hypersurface.

One of the main advantages offered by our approach is a generalization of material parameters and geometric configuration. We tested our numerical treatment of the quartic eigenvalue problem with analytical predictions in the case of an isotropic medium, and observed excellent agreement. We assessed the relative strength of computed eigenmodes by quantifying eigenvalues via a quality factor, and demonstrated using concrete examples that it is possible to achieve a better quality factor. An improved quality factor is observed for both gradient-index waveguide and generalized geometry.

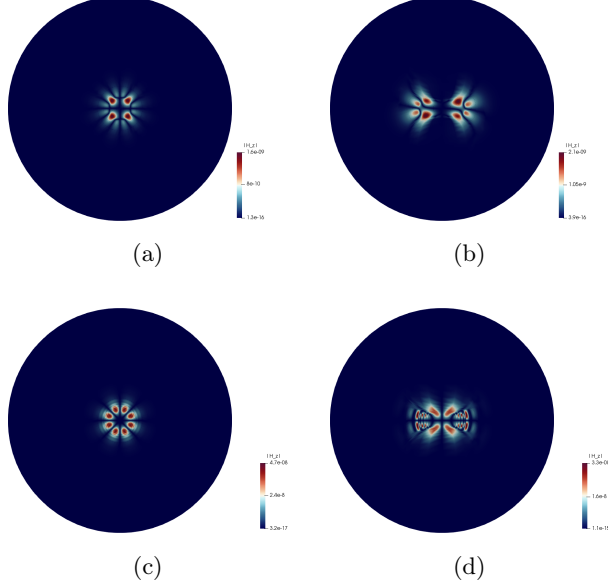


Figure 6: An example of $|H_z|$ eigenmode before and after mesh deformation. (a) & (b) are obtained using $\varepsilon_{r,1}$ with modal order of $m = 4$ and (c) & (d) via $\varepsilon_{r,2}$ with $m = 4$.

Ideally, we wish to solve the following optimization problem:

$$\begin{aligned}
& \underset{\varepsilon_r(\mathbf{x}), \mu_r(\mathbf{x}), \Sigma}{\text{maximize}} && \text{Re } k_z(\varepsilon_r(\mathbf{x}), \mu_r(\mathbf{x}), \Sigma) / \text{Im } k_z(\varepsilon_r(\mathbf{x}), \mu_r(\mathbf{x}), \Sigma) \\
& \text{subject to} && [\varepsilon_r]_{\Sigma} = [\mu_r]_{\Sigma} = 0, \text{ with regularity assumptions,} \\
& && l(\Sigma) = c, \text{ where } c \text{ is constant.}
\end{aligned}$$

Here, $l(\cdot)$ denotes the length of the curve. In the special case where $\varepsilon_r \equiv 1$ and Σ is two infinite parallel layers, the optimization problem reduces to one discussed in [28]. We observe that these generalized constraints can be used as a basis for solving related shape optimization problems for complicated multilayer optical devices, which is the subject of future research.

Appendix A. Derivation of the weak form

In this appendix, we carry out in detail the derivation of our weak formulation (9). As a preliminary step, we explain how the longitudinal component of the guided mode is derived.

Appendix A.1. Longitudinal component

The transverse and the longitudinal components of the rescaled time-harmonic Maxwell's equations with $e^{ik_z z}$ dependence are

$$(A.1) \quad \begin{cases} i\mu_r \mathbf{H}_s = \nabla_s \times \hat{z} E_z + ik_z \hat{z} \times \mathbf{E}_s, \\ -i\varepsilon_r \mathbf{E}_s = \nabla_s \times \hat{z} H_z + ik_z \hat{z} \times \mathbf{H}_s, \end{cases}$$

$$(A.2) \quad \begin{cases} \nabla_s \times \mathbf{E}_s = i\mu_r \hat{z} H_z, \\ \nabla_s \times \mathbf{H}_s = -i\varepsilon_r \hat{z} E_z. \end{cases}$$

and the corresponding jump conditions at an interface Σ are

$$(A.3) \quad \begin{cases} [\boldsymbol{\nu} \times (\mathbf{H}_s + \hat{z} H_z)]_\Sigma = \sigma_r^\Sigma \left\{ (\boldsymbol{\nu} \times (\mathbf{E}_s + \hat{z} E_z)) \times \boldsymbol{\nu} \right\}_\Sigma, \\ [\boldsymbol{\nu} \cdot \mu_r (\mathbf{H}_s + \hat{z} H_z)]_\Sigma = [\boldsymbol{\nu} \times (\mathbf{E}_s + \hat{z} E_z)]_\Sigma = [\boldsymbol{\nu} \cdot \varepsilon_r (\mathbf{E}_s + \hat{z} E_z)]_\Sigma = 0, \end{cases}$$

where $\boldsymbol{\nu}$ is the normal vector at Σ . Equate each component of (A.3) to obtain

$$(A.4) \quad \begin{cases} [(\mathbf{H}_s \cdot \boldsymbol{\tau}) \hat{z}]_\Sigma = \sigma_r^\Sigma \left\{ (-E_z \boldsymbol{\tau}) \times \boldsymbol{\nu} \right\}_\Sigma = \sigma_r^\Sigma E_z \hat{z} \Big|_\Sigma, \\ [-H_z \boldsymbol{\tau}]_\Sigma = \sigma_r^\Sigma \left\{ (\mathbf{E}_s \cdot \boldsymbol{\tau}) \hat{z} \times \boldsymbol{\nu} \right\}_\Sigma = \sigma_r^\Sigma (\mathbf{E}_s \cdot \boldsymbol{\tau}) \boldsymbol{\tau} \Big|_\Sigma, \\ [\varepsilon_r \mathbf{E}_s]_\Sigma \cdot \boldsymbol{\nu} = [\mu_r \mathbf{H}_s]_\Sigma \cdot \boldsymbol{\nu} = [\mathbf{E}_s]_\Sigma \cdot \boldsymbol{\tau} = [E_z]_\Sigma = 0. \end{cases}$$

Substitute one of (A.1) into the other to obtain (A.5).

$$(A.5) \quad \begin{cases} k_s^2 \mathbf{E}_s = i(k_z \nabla_s E_z + \mu_r \nabla_s \times H_z), \\ k_s^2 \mathbf{H}_s = i(k_z \nabla_s H_z - \varepsilon_r \nabla_s \times E_z). \end{cases}$$

The second-order time-harmonic Maxwell's equations are

$$(A.6) \quad \begin{aligned} (\nabla_s + ik_z \hat{z}) \times (\mu_r^{-1} (\nabla_s + ik_z \hat{z}) \times \mathbf{E}) - \varepsilon_r \mathbf{E} &= 0, \\ (\nabla_s + ik_z \hat{z}) \times (\varepsilon_r^{-1} (\nabla_s + ik_z \hat{z}) \times \mathbf{H}) - \mu_r \mathbf{H} &= 0, \end{aligned}$$

Equate the z -component of (A.6) to obtain (5).

Appendix A.2. Derivation of the weak form

We multiply (6) by k_s^4 and distribute it in a particular manner that eases the handling of the inhomogeneities.

$$(A.7) \quad \begin{cases} -k_s^4 \left(\left(\nabla_s \frac{1}{k_s^2} \right) \cdot (\varepsilon_r \nabla_s E_z) + \frac{1}{k_s^2} \nabla_s \cdot (\varepsilon_r \nabla_s E_z) \right) \\ \quad - k_z k_s^4 \left(\left(\nabla_s \frac{1}{k_s^2} \right) \cdot (\nabla_s \times \hat{z} H_z) \right) - \varepsilon_r k_s^4 E_z = 0 \\ -k_s^4 \left(\left(\nabla_s \frac{1}{k_s^2} \right) \cdot (\mu_r \nabla_s H_z) + \frac{1}{k_s^2} \nabla_s \cdot (\mu_r \nabla_s H_z) \right) \\ \quad + k_z k_s^4 \left(\left(\nabla_s \frac{1}{k_s^2} \right) \cdot (\nabla_s \times \hat{z} E_z) \right) - \mu_r k_s^4 H_z = 0. \end{cases}$$

Since $\nabla_s k_s^{-2} = -k_s^{-4} \nabla_s k_s^2$, some algebra shows that the expression in the first line of (A.7) is equivalent to

$$(A.8) \quad \begin{aligned} & -k_s^4 \left(\left(\nabla_s \frac{1}{k_s^2} \right) \cdot (\varepsilon_r \nabla_s E_z) + \frac{1}{k_s^2} \nabla_s \cdot (\varepsilon_r \nabla_s E_z) \right) \\ & = \nabla_s k_s^2 \cdot (\varepsilon_r \nabla_s E_z) - k_s^2 \nabla_s \cdot (\varepsilon_r \nabla_s E_z) \\ & = \nabla_s \cdot (k_s^2 (\varepsilon_r \nabla_s E_z)) - 2k_s^2 \nabla_s \cdot (\varepsilon_r \nabla_s E_z). \end{aligned}$$

Additionally, we note that the curl terms in (A.7) can be written as

$$(A.9) \quad \begin{aligned} & -k_z k_s^4 \left(\left(\nabla_s \frac{1}{k_s^2} \right) \cdot (\nabla_s \times \hat{z} H_z) + \frac{1}{k_s^2} \nabla_s \cdot (\nabla_s \times \hat{z} H_z) \right) \\ & = k_z \nabla_s k_s^2 \cdot (\nabla_s \times \hat{z} H_z) - k_z k_s^2 \nabla_s \cdot (\nabla_s \times \hat{z} H_z) \\ & = k_z \nabla_s \cdot (k_s^2 (\nabla_s \times \hat{z} H_z)) - 2k_z k_s^2 \nabla_s \cdot (\nabla_s \times \hat{z} H_z). \end{aligned}$$

Even though the last term vanishes, we keep it, as it will be later utilized to express the interface contribution nicely.

We now test with smooth functions φ and ψ , and integrate by parts to arrive at

$$(A.10) \quad \begin{aligned} & - (k_s^2 \varepsilon_r \nabla_s E_z, \nabla_s \varphi) + 2(\varepsilon_r \nabla_s E_z, \nabla_s (\bar{k}_s^2 \varphi)) - k_z (k_s^2 \nabla_s \times \hat{z} H_z, \nabla_s \varphi) \\ & \quad + 2k_z (\nabla_s \times \hat{z} H_z, \nabla_s (\bar{k}_s^2 \varphi)) - (\varepsilon_r k_s^4 E_z, \varphi) \\ & - (k_s^2 \mu_r \nabla_s H_z, \nabla_s \psi) + 2(\mu_r \nabla_s H_z, \nabla_s (\bar{k}_s^2 \psi)) + k_z (k_s^2 \nabla_s \times \hat{z} E_z, \nabla_s \psi) \\ & \quad - 2k_z (\nabla_s \times \hat{z} E_z, \nabla_s (\bar{k}_s^2 \psi)) - (\mu_r k_s^4 H_z, \psi) \\ & + \langle [k_s^2 \varepsilon_r \partial_\nu E_z + k_s^2 k_z \partial_\tau H_z]_\Sigma, \varphi \rangle_\Sigma + \langle [k_s^2 \mu_r \partial_\nu H_z - k_s^2 k_z \partial_\tau E_z]_\Sigma, \psi \rangle_\Sigma. \end{aligned}$$

Using (3), (7), and (A.5), the interface contributions simplify to

$$(A.11) \quad \langle [k_s^2(\varepsilon_r \partial_\nu E_z + k_z \partial_\tau H_z)]_\Sigma, \varphi \rangle_\Sigma + \langle [k_s^2(\mu_r \partial_\nu H_z - k_z \partial_\tau E_z)]_\Sigma, \psi \rangle_\Sigma \\ = -i \langle [k_s^4 \mathbf{H}_\tau]_\Sigma, \varphi \rangle_\Sigma - i \langle [k_s^4 \mathbf{E}_\tau]_\Sigma, \psi \rangle_\Sigma = -i \sigma_r^\Sigma \langle k_s^4 E_z, \varphi \rangle_\Sigma.$$

Expand the $\nabla_s(\bar{k}_s^2 \varphi)$ and $\nabla_s(\bar{k}_s^2 \psi)$ to arrive at

$$(A.12) \quad (\mu_r \varepsilon_r^2 \nabla_s E_z, \nabla_s \varphi) + 2(\varepsilon_r \nabla_s E_z, \nabla_s(\bar{\varepsilon}_r \bar{\mu}_r) \varphi) \\ + k_z(\mu_r \varepsilon_r \nabla_s \times \hat{z} H_z, \nabla_s \varphi) - k_z^2(\varepsilon_r \nabla_s E_z, \nabla_s \varphi) \\ + 2k_z(\nabla_s \times \hat{z} H_z, \nabla_s(\bar{\varepsilon}_r \bar{\mu}_r) \varphi) - k_z^3(\nabla_s \times \hat{z} H_z, \nabla_s \varphi) - (\varepsilon_r k_s^4 E_z, \varphi) \\ + (\varepsilon_r \mu_r^2 \nabla_s H_z, \nabla_s \psi) + 2(\mu_r \nabla_s H_z, \nabla_s(\bar{\varepsilon}_r \bar{\mu}_r) \psi) \\ - k_z(\mu_r \varepsilon_r \nabla_s \times \hat{z} E_z, \nabla_s \psi) - k_z^2(\mu_r \nabla_s H_z, \nabla_s \psi) \\ - 2k_z(\nabla_s \times \hat{z} E_z, \nabla_s(\bar{\varepsilon}_r \bar{\mu}_r) \psi) + k_z^3(\nabla_s \times \hat{z} E_z, \nabla_s \psi) - (\mu_r k_s^4 H_z, \psi) \\ - i \sigma_r^\Sigma \langle k_s^4 E_z, \varphi \rangle_\Sigma = 0.$$

References

- [1] K. S. Novoselov, S. V. M. A. K. Geim, D. Jiang, Y. Zhang, S. V. Dubonos, I. V. Grigorieva, A. A. Firsov, Electric field effect in atomically thin carbon films, *Science* 306 (2004) 666.
- [2] Y. V. Bludov, A. Ferreira, N. M. R. Peres, M. I. Vasileskiy, A primer on surface plasmon-polaritons in graphene, *International Journal of Modern Physics* 27 (10) (2013) 1341001.
- [3] J. Liu, X. Zhai, L.-L. Wang, H.-J. Li, F. Xie, Q. Lin, S.-X. Xia, Analysis of mid-infrared surface plasmon modes in a graphene-based cylindrical hybrid waveguide, *Plasmonics* 11 (2016) 703–711.
- [4] R. F. Oulton, V. J. Sorger, T. Zentgraf, R.-M. Ma, C. Gladden, L. Dai, G. Bartal, X. Zhang, Plasmon lasers at deep subwavelength scale, *Nature Letters* 461 (2009) 629–632.
- [5] A. Vakil, N. Engheta, Transformation optics using graphene, *Science* 332 (2011) 1291.
- [6] B. Gavin, A. Miedlar, E. Polizzi, Feast eigensolver for nonlinear eigenvalue problems, *Journal of Computational Science* 27 (2018) 107–117.

- [7] J. Gopalakrishnan, L. Grubisic, J. Owall, B. Q. Parker, Analysis of feast spectral approximations using the dpg discretization, *Computational Methods in Applied Mathematics* 19 (2019) 251–266.
- [8] J. Gopalakrishnan, L. Grubisic, J. Owall, Spectral discretization errors in filtered subspace iteration, *Mathematics of Computation* 89 (2020) 321.
- [9] Z. Bai, D. Lu, B. Vandereycken, Robust rayleigh quotient minimization and nonlinear eigenvalue problems, *Siam Journal on Scientific Computing* 40 (2018) A3495–A3522.
- [10] D. Arndt, W. Bangerth, T. C. Clevenger, D. Davydov, M. Fehling, D. Garcia-Sanchez, G. Harper, T. Heister, L. Heltai, M. Kronbichler, R. M. Kynch, M. Maier, J.-P. Pelteret, B. Turcksin, D. Wells, The `deal.II` library, version 9.1, *Journal of Numerical Mathematics* Accepted (2019). doi:10.1515/jnma-2019-0064.
URL <https://dealii.org/deal91-preprint.pdf>
- [11] S. Balay, K. Buschelman, V. Eijkhout, W. D. Gropp, D. Kaushik, M. G. Knepley, L. C. McInnes, B. F. Smith, H. Zhang, *Petsc users manual*, Technical Report ANL-95/11 - Revision 2.1.5 Argonne National Laboratory (2004).
- [12] V. Hernandez, J. E. Roman, V. Vidal, A scalable and flexible toolkit for the solution of eigenvalue problems, *ACM Transactions on Mathematical Software* 31 (2005).
- [13] F. D. Teran, F. M. Dopico, D. S. Mackey, Spectral equivalence of matrix polynomials and the index sum theorem, *Linear Algebra and its Applications* 459 (2014).
- [14] J. Xu, N. Shi, Y. Chen, X. Lu, H. Wei, Y. Lu, N. Liu, B. Zhang, J. Wang, Tm01 mode in a cylindrical hybrid plasmonic waveguide with large propagation length, *Applied Optics* 57 (2018) 4043–4047.
- [15] Y. Gao, G. Ren, B. Zhu, H. Liu, Y. Lian, S. Jian, Analytical model for plasmon modes in graphene-coated nanowire, *Optics Express* 22 (2014) 24322–24331.
- [16] Y. Gao, G. Ren, B. Zhu, J. Wang, S. Jian, Single-mode graphene-coated nanowire plasmonic waveguide, *Optics Letters* 39 (2014) 5909–5912.

- [17] Y. Xu, Y. Fu, H. Chen, Planar gradient metamaterials, *Nature Reviews Materials* 1 (2016) 16067.
- [18] F. Moharrami, Z. Atlasbaf, Tunable grin lensing based on graphene-dielectric multilayer metamaterials, *Journal of Optics* 22 (2020).
- [19] Q. I. Dai, Y. H. Lo, W. C. Chew, L. J. Jiang, An efficiently preconditioned eigenanalysis of inhomogeneously loaded rectangular cavities, *IEEE Antennas Wireless Propagation Letters* 12 (2013) 58–61.
- [20] Q. I. Dai, W. C. Chew, L. J. Jiang, Differential forms inspired discretization for finite element analysis of inhomogeneous waveguides, *Progress in Electromagnetics Research* 143 (2013) 745–760.
- [21] W. C. Chew, *Waves and Fields in Inhomogeneous Media*, Wiley-IEEE Press, New York, 1999.
- [22] D. A. White, J. M. Koning, Computing solenoidal eigenmodes of the vector helmholtz equation: A novel approach, *IEEE Transactions on Magnetism* 38 (2002) 3420–3425.
- [23] E. Polizzi, Density-matrix-based algorithms for solving eigenvalue problems, *Physics Review B* 79 (2009) 115112.
- [24] M. Maier, D. Margetis, M. Luskin, Dipole excitation of surface plasmon on a conducting sheet: finite element approximation and validation, *Journal of Computational Physics* 339 (2017) 126–145.
- [25] F. Collino, P. Monk, The perfectly matched layer in curvilinear coordinates, *SIAM Journal on Scientific Computing* 19 (1998) 2061–2090.
- [26] P. Monk, *Finite Element Methods for Maxwell’s Equations*, Numerical Mathematics and Scientific Computation, Oxford University Press, 2003.
- [27] D. S. Mackey, N. Mackey, C. Mehl, V. Mehrmann, Möbius transformations of matrix polynomials, *Linear Algebra and its Applications* 470 (2014) 120–184.
- [28] J. Song, M. Maier, M. Luskin, Adaptive finite element simulations of waveguide configurations involving parallel 2d material sheets, *Computer Methods in Applied Mechanics and Engineering* 351 (2019) 20–34.